# Response-Based Frequency Stability Assessment under Multi-Scale Disturbances in High-Renewable Power Systems

Jinhui Chen, Huadong Sun, Senior Member, IEEE, Fellow, CSEE, Ping Wu, Baocai Wang, and Bing Zhao, Senior Member, IEEE

Abstract-In high-renewable power systems, active-power disturbances are becoming larger and exhibit increasingly diverse time scales, which complicates frequency stability assessment under unanticipated events. This paper presents a response-based frequency stability assessment method that uses disturbance power, inferred from generator electrical responses, to provide a unified treatment of multi-scale disturbances. Unanticipated disturbances are first classified into short-term and permanent events; permanent disturbances are further divided into step, second-level slope and minute-level slope disturbances. Based on the measured power responses of generator groups, a unified disturbance-power model is constructed to identify the disturbance type online and to quantify disturbance intensity through the disturbance power and its rate of change. Analytical frequency-response models are then derived for each disturbance class. For step disturbances, the maximum tolerable disturbance power is obtained under steady-state and transient frequency deviation constraints, and a safety-margin index is defined. For slope-type disturbances, an improved system frequency response (SFR) model and the rotor motion equation after exhaustion of primary frequency regulation are used to compute the over-limit time of frequency deviation. The proposed response-based assessment method is validated on the CSEE-FS frequencystability benchmark system, demonstrating its effectiveness and accuracy for quantitative frequency stability assessment in highrenewable power systems.

Index Terms—Response-based assessment, disturbance power, multi-scale disturbances, frequency stability, high-renewable power systems.

# I. INTRODUCTION

Which the large-scale integration of renewable generation and DC transmission into power systems, synchronous inertia and conventional primary frequency-regulation resources are continuously decreasing. This deterioration of frequency response under disturbances poses a serious threat to secure system operation [1], [2]. At the same time, the scale and complexity of active-power disturbances are increasing, which aggravates the risk of cascading failures and brings new challenges to frequency-security control [3], [4].

For conventional step disturbances of known magnitude, extensive research has been conducted on the calculation of

frequency indicators and the quantification of system inertia requirements. The classical SFR model in [5] provides analytical expressions for frequency indicators and reveals their influencing factors. For high-renewable power systems, the SFR model has been extended to incorporate various frequency-support resources [6]. In [7], [8], the primary frequency-regulation characteristic of generators is linearized to obtain simplified analytical formulas for the maximum frequency deviation. Inertia estimation and minimum inertia requirement evaluation methods have been proposed in [9] -[11], while [12], [13] investigate virtual inertia control using wind turbine kinetic energy and DC capacitors. The minimum synchronous inertia requirement in renewable power systems is analyzed in [14], and the theoretical foundations and modelling issues of frequency stability are systematically reviewed in [15]. Furthermore, [16] incorporates frequency security constraints into unit commitment for converter-based generators.

Most of the above studies focus on single step disturbances that cause permanent power imbalance. However, recent frequency stability events have shown that, in addition to step disturbances caused by DC blocking or generator tripping [14] - [16], short-term disturbances and time-varying slope disturbances can also play a critical role. Short-term disturbances are typically associated with DC commutation failures or low-voltage ride-through (LVRT) of renewable generation. Time-varying slope disturbances can be further divided by time scale into second-level slope disturbances caused by cascading outages and minute-level slope disturbances caused by continuous load growth. For example, during the 9 August 2019 frequency event in Great Britain, a combination of wind farms, conventional units and distributed resources tripped sequentially under extreme weather conditions, leading to a rapid increase in frequency deviation within several seconds and triggering low-frequency load shedding [17], [18]. In another case, in September 2021, the load in Northeast China increased slowly over time, creating a persistent supply-demand gap. When the frequency fell to 49.8 Hz, all available frequency-regulation measures had been exhausted and emergency load shedding had to be

This work was supported by the National Natural Science Foundation of China (U2166601). J. H. Chen, H. D. Sun (corresponding author, email: sunhd@epri.sgcc.com.cn), P. W, B. C. Wang and B. Zhao are with the State

Key Laboratory of Power Grid Safety and Energy Conservation, China Electric Power Research Institute, Beijing 100192, China.

implemented. Unlike second-level slope disturbances, minutelevel slope disturbances have smaller power-change slopes but longer duration, causing a slow yet continuous deterioration of frequency deviation.

In summary, frequency analysis methods designed for single, anticipated step disturbances are no longer adequate for quantitatively discriminating frequency stability under emerging disturbance forms. There is still a lack of responsebased quantitative methods to identify unanticipated step disturbances, and systematic research on the classification and quantification of frequency response under time-varying disturbances is even rarer. With the development of synchrophasor and wide-area measurement technologies, electrical quantities in power systems can be measured accurately and synchronously. Response-based online analysis has already been applied to oscillation source location and voltage stability control [19], [20]. Building on such measurement capabilities, recent studies have demonstrated system-level inertia estimation using ambient frequency data [21], assessment and enhancement of frequency-response capability considering thermal-unit dynamic conditions [22], communication-resource allocation schemes to reduce the time delay of frequency-regulation services [23], and wide-area active frequency-control strategies based on multi-step-size model predictive control [24]. These advances highlight the need for response-based, quantitative tools that can directly link disturbance characteristics extracted from measured responses with frequency-stability margins in high-renewable power systems.

Motivated by the distinct response mechanisms of different disturbance types and time scales, this paper presents a response-based frequency stability assessment method under multi-scale unanticipated disturbances. Using generator electrical response data as the basic input, the method first classifies unanticipated disturbances into disturbances. step disturbances, second-level disturbances and minute-level slope disturbances, establishes unified quantitative indicators of disturbance intensity based on disturbance power and its rate of change inferred from the responses. Then, by combining the SFR model with the primary frequency regulation of synchronous and power electronic units, and by considering the exhaustion of primary frequency-regulation capacity, analytical criteria are derived to determine the maximum tolerable disturbance power and the over-limit time of frequency deviation under different disturbance types. Finally, the proposed response-based method is validated on the CSEE-FS frequency-stability benchmark system [25] under typical disturbance scenarios, demonstrating its accuracy and practicality for online frequency-stability assessment and active prevention and control in high-renewable power systems.

### II. DISTURBANCE TYPE CLASSIFICATION AND IDENTIFICATION

# A. Disturbance Scenario Classification

Unanticipated disturbances are first classified into short-term and permanent disturbances.

A short-term disturbance is mathematically represented by a step increase in disturbance power, followed by a ramp decrease with a given slope after the fault duration. Its severity is characterized jointly by the magnitude of the disturbance power and the fault duration.

Permanent disturbances are further divided into three categories:

- 1) Step disturbance. The disturbance power experiences a sudden increase at a certain instant and then remains approximately constant. It can be modelled by a step function, and its severity is quantified by the magnitude of the disturbance power.
- 2) Second-level slope disturbance. The disturbance power starts to increase linearly from zero at a certain instant and can be modelled by a ramp function. Its characteristic feature is that the disturbance power changes rapidly, and the time scale for reaching the transient frequency deviation limit is on the order of seconds. The severity of this type of disturbance is characterized by the rate of change of disturbance power.
- 3) Minute-level slope disturbance. This type can also be modelled by a ramp function, but the disturbance power changes slowly and the time scale for reaching the frequency deviation limit is on the order of minutes. Its severity is likewise characterized by the rate of change of disturbance power.

Following a disturbance, the system frequency response can be divided into three stages. In the first stage, the power imbalance is redistributed among generators according to their electrical distance and initial power-angle differences, leading to corresponding increases or decreases in electromagnetic power. In the second stage, primary frequency regulation of generators and frequency-dependent loads is activated, gradually offsetting the power imbalance. In the third stage, secondary frequency regulation and tertiary controls restore the frequency to its nominal value.

For step disturbances and second-level slope disturbances, the total power imbalance grows rapidly during the early stage. This feature is used to identify these two types of disturbances in a response-based manner. The total unbalanced power of the system is first obtained from the variations in electromagnetic power of each generating unit, from which the disturbance power (for step disturbances) and the rate of change of disturbance power (for second-level slope disturbances) are evaluated. These events are further classified as short-term disturbances if the disturbance power subsequently returns to its pre-disturbance level within a short time.

For minute-level slope disturbances, the disturbance power increases slowly and does not exceed the predefined power threshold in the early stage. The system frequency therefore drifts downward continuously and slowly until the available primary frequency-regulation capacity of the generators is exhausted and the frequency deviation surpasses its threshold. In this case, the rate of change of disturbance power is determined from the generator primary frequency-regulation limits and the power-balance condition at the frequency deviation threshold.

### B. Identification of disturbance type

To accurately distinguish the four types of disturbances, appropriate power and frequency deviation thresholds must be set according to the system operating condition.

The power threshold is designed to avoid misclassifying minute-level slope disturbances as step or second-level slope disturbances. To this end, the maximum disturbance power that a minute-level slope disturbance can produce within the unbalanced power-distribution interval is calculated and used as the power threshold.

The rates of change of disturbance power for second-level and minute-level slope disturbances are summarized in Table I. Let  $k_1$  denote the critical slope separating second-level and minute-level slope disturbances, and let T be the unbalanced power distribution time. For a minute-level slope disturbance, the maximum disturbance power attainable within T is  $k_1T$ ; therefore, the power threshold is set as  $\Delta P_{\rm sh} = k_1T$ .

TABLE I RANGES OF DISTURBANCE-POWER SLOPE FOR SECOND-LEVEL AND MINUTE-LEVEL SLOPE DISTURBANCES

Disturbance type	Range of disturbance-power slope	
second-level slope disturbance	$k > k_1$	
minute-level slope disturbance	$0 \le k \le k_1$	

The schematic for setting the power threshold is illustrated in Fig. 1. If  $\Delta P > \Delta P_{\rm sh}$  within time T, the disturbance is identified as either a step disturbance or a second-level slope disturbance. The specific type is then determined based on whether the disturbance power is time-varying: a time-varying disturbance power indicates a second-level slope disturbance, whereas a constant disturbance power indicates a step disturbance. The event is classified as a short-term disturbance if the disturbance power subsequently decreases rapidly and returns close to its pre-disturbance value.

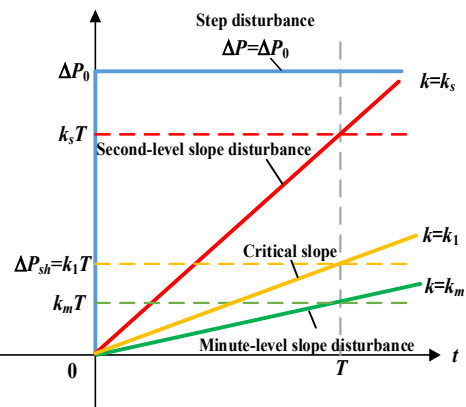


Fig. 1. Schematic diagram for setting the disturbance-power threshold  $\Delta P_{\rm sh}$ .

The frequency deviation threshold is defined as the frequency deviation at which the primary frequency-regulation capacity of the generators is fully exhausted.

Assume that the primary frequency-regulation capacity of the generator accounts for a proportion m of their total capacity, and that new energy resources provide a proportion n. When the generator primary frequency-regulation capacity is fully utilized, the corresponding frequency deviations can be expressed as (1) and (2):

$$\Delta f_G = \frac{mP_{GN} + nP_{NEW}}{(K_G + K_w)S_N} f_N \tag{1}$$

$$\Delta f_{\rm sh} = \Delta f_{\rm G} + f_{\rm d} \tag{2}$$

where  $\Delta f_{\rm G}$  is the steady-state frequency deviation resulting from generator regulation,  $K_{\rm G}$  and  $K_{\rm w}$  are the unit regulation gains of the generators and the new-energy resources, respectively,  $P_{\rm GN}$  and  $P_{\rm NEW}$  are the rated capacities of the generators and new-energy resources, respectively,  $f_{\rm d}$  the frequency deviation at which primary frequency control is activated, and  $\Delta f_{\rm sh}$  denotes the total frequency deviation when the primary frequency regulation capacity of the generators is exhausted.

When  $\Delta f > \Delta f_{\rm sh}$  and the disturbance power does not reach the power threshold, the disturbance can be identified as a minute-level slope disturbance.

As an example, consider the parameter set:  $K_{\rm G}$ =20,  $K_{\rm w}$ =10,  $K_{\rm L}$ =1, H=4,  $P_{\rm GN}$ =1000MW,  $P_{\rm NEW}$ =1000MW,  $f_{\rm d}$ =0.033Hz, m=0.06, n=0.1. Suppose that the time required for a minute-level slope disturbance to reach the frequency-activation threshold exceeds 30 s. The corresponding critical slope is then  $k_1$ =3MW/s, meaning that the disturbance power increases at a rate of 0.15% of the system capacity per second. If the unbalanced power distribution time is T=0.5s, the resulting power threshold is  $\Delta P_{\rm sh}$ =1.5MW, and the frequency deviation threshold is  $\Delta f_{\rm sh}$ =0.3Hz.

#### III. QUANTIFICATION OF DISTURBANCE INTENSITY

### A. Short-Term Disturbances and Step Disturbances

For short-term disturbances and step disturbances, the disturbance intensity is quantified by the magnitude of the disturbance power  $\Delta P_0$ . When a disturbance occurs, the total power imbalance at the centre of inertia is allocated to the electromagnetic power of each generator in the area as:

$$\Delta P_0 = \sum_{i=1}^n \Delta P_{ei} \tag{3}$$

After linearization, the change in electromagnetic power of generator i can be expressed as:

$$\Delta P_{ei} = \sum_{\substack{j=1\\j\neq i,k}}^{n} E_i E_j B_{ij} \cos \delta_{ij} \Delta \delta_{ij} + U_p E_i B_{ip} \cos \delta_{ip} \Delta \delta_{ip}$$
 (4)

where  $E_i$  and  $E_j$  are the internal voltages of generator i and j,  $U_p$  is the voltage at the disturbance point,  $\delta_{ij}$  is the power-angle difference between generators i and j,  $\delta_{ip}$  is the power-angle difference between generator i and the disturbance point, and  $B_{ij}$  and  $B_{ip}$  are the network susceptance between generators and between generator i and the disturbance point, respectively.

Since all generators remain synchronized in the initial stage of the disturbance, we have  $\delta_i$ =0, and (4) reduces to:

$$\Delta P_{ei} = U_p E_i B_{ip} \cos \delta_{ip} \Delta \delta_{ip} \tag{5}$$

Combining (3) and (5), the disturbance power  $\Delta P_0$  can be calculated from measurable quantities such as the voltage magnitude and phase angles at each generator and at the disturbance point, yielding:

$$\Delta P_0 = \sum_{i=1}^n U_p E_i B_{ip} \cos \delta_{ip} \Delta \delta_{ip}$$
 (6)

Thus, the intensity of short-term and step disturbances can be

obtained in a response-based manner from the generator electrical responses.

### B. Second-level Slope Disturbances

For second-level slope disturbances, the disturbance intensity is characterized by the disturbance-power slope, denoted by  $k_s$ .

When the disturbance power varies linearly with time and the disturbance inception is taken as the time origin, it can be expressed as  $\Delta P_0 = k_s t$ . Substituting this relation into (6) yields

$$k_s t = \sum_{i=1}^n U_p E_i B_{ip} \cos \delta_{ip} \Delta \delta_{ip} \tag{7}$$
 From (7), the disturbance-power slope for a second-level

slope disturbance can be obtained as

$$k_{s} = \frac{\sum_{i=1}^{n} U_{p} E_{i} B_{ip} \cos \delta_{ip} \Delta \delta_{ip}}{t}$$
 (8)

Hence, ks can be quantified directly from the measured generator voltages and phase angles, providing a responsebased index of disturbance intensity for second-level slope disturbances.

### C. Minute-level Slope Disturbances

For minute-level slope disturbances, the disturbance intensity is quantified by the rate of change of disturbance power  $k_{\rm m}$ .

Owing to the much longer time scale of frequency evolution in this case, it is assumed that, by the time the frequency deviation reaches its threshold, the power imbalance has been fully compensated by the primary frequency regulation of generators and loads. The value of  $k_{\rm m}$  can therefore be determined from the power-balance condition at the frequency deviation threshold.

When the frequency deviation reaches the starting threshold  $\Delta f_{\rm sh}$ , the load-frequency damping response (i.e., load regulation power) is:

$$\Delta P_L = K_L \Delta f_{sh} \tag{9}$$

where  $K_L$  is the load damping coefficient of the system.

Let  $t_1$  denote the instant when the frequency deviation first reaches  $\Delta f_{\rm sh}$ . Applying the power balance condition at  $t_1$  yields:

$$k_m t_1 = \Delta P_L + m P_{GN} + n P_{New} \tag{10}$$

Combining (9) and (10), the disturbance-power slope for a minute-level slope disturbance can be calculated as:

$$k_m = \frac{K_L \Delta f_{sh} + mP_{GN} + nP_{New}}{t_1} \tag{11}$$

This provides a quantitative measure of disturbance intensity for minute-level slope disturbances based on the primary frequency regulation limits and the frequency deviation threshold.

### IV. FREQUENCY STABILITY DISCRIMINATION

### A. Short-Term Disturbances

For short-term power disturbances, the response of primary frequency control is delayed and the initial frequency dynamics are dominated by the inertial response of synchronous generators. The corresponding process of energy accumulation is illustrated in Fig. 2.

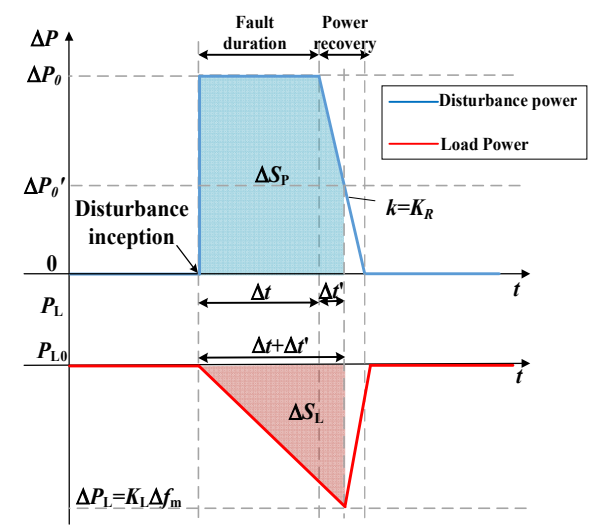


Fig. 2. Accumulated energy due to disturbance power and load-frequency modulation during a short-term disturbance.

At the instant when the frequency deviation reaches its maximum, the accumulated energies associated with the disturbance power and the load-frequency modulation are given by (12) and (13), respectively:

$$\Delta S_{\rm P} = \frac{(2\Delta P_0 - \Delta P_0')(\Delta t + \Delta t')}{2} \tag{12}$$

$$\Delta S_{\rm L} = \frac{K_{\rm L} \Delta f_{\rm m}^* P_{\rm L0}(\Delta t + \Delta t')}{2} \tag{13}$$

where  $\Delta P_0$  is the disturbance power at the time of maximum frequency deviation,  $\Delta t$  is the fault duration,  $\Delta P_0$  is the residual disturbance power at the instant when the frequency deviation reaches its maximum,  $\Delta t'$  is the time interval from disturbance clearance to the instant when the frequency deviation reaches its maximum, with  $\Delta P_0' = K_R \Delta t'$ ,  $P_{L0}$  is the pre-disturbance load power,  $\Delta f_{\rm m}$  is the maximum transient frequency deviation; and  $K_{\rm R}$  is the power recovery rate.

The minimum kinetic energy required by the system is expressed as:

$$W_{k} = \frac{\left(\frac{(2\Delta P_{0} - \Delta P_{0}')(\Delta t + \Delta t')}{2} - \frac{K_{L}\Delta f_{m}^{*} P_{L0}(\Delta t + \Delta t')}{2}\right)}{2\Delta f_{m}^{*}}$$
(14)

When the frequency deviation reaches its maximum, the power imbalance  $\Delta P_0$  is fully compensated by the inertial response and load-frequency modulation:

$$\Delta P_0 = K_R \Delta t' + K_L \Delta f_m^* P_{L0} \tag{15}$$

Combining (14) and (15), and denoting the transient frequency deviation limit by  $\Delta f_{\text{max}}$ , the critical disturbance power for a short-term disturbance is obtained as:

$$\frac{\Delta P_{\text{max}}^{2}}{K_{R}} + \Delta P_{\text{max}} \left( \Delta t - \frac{K_{L}}{K_{R}} P_{\text{L0}} \Delta f_{\text{max}}^{*} \right) - 4H \Delta f_{\text{max}}^{*} P_{\text{G}} = 0 \quad (16)$$

(16) provides a quantitative criterion for assessing whether a short-term disturbance will cause the transient frequency deviation to exceed its limit.

### B. Step Disturbances

1) Critical Disturbance Power Under Steady-State Frequency **Deviation Constraint** 

The steady-state frequency deviation is determined by the primary frequency regulation of generators and the frequency sensitivity of loads. The corresponding unit regulation powers are characterized by the regulation gains of generators and loads.

When the frequency settles to a new steady-state value, the power imbalance equals the sum of the load regulation power and the generator regulation power, namely:

$$\Delta P_{\text{max 1}} = \frac{K_L \Delta f_{ss} P_{L0} + K_G \Delta f_{ss} P_{GN} + K_w \Delta f_{ss} P_{NEW}}{f_N}$$
(17)

where  $\Delta f_{\rm ss}$  is the steady-state frequency deviation limit,  $f_{\rm N}$  is the nominal system frequency (50 Hz), and  $\Delta P_{\rm max1}$  is the critical disturbance power under the steady-state frequency deviation constraint.

Because the generator frequency regulation capacity is limited by the prime mover, once this capacity is exhausted, any additional power imbalance must be absorbed solely by load-frequency regulation. The corresponding power-balance condition is:

$$\Delta P_{\max 2} = mP_{GN} + nP_{NEW} + \frac{K_L \Delta f_{ss} P_{L0}}{f_N}$$
 (18)

The smaller of the two values obtained from (17) and (18) is taken as the maximum disturbance power that the system can withstand under the steady-state frequency-deviation constraint.

2) Critical Disturbance Power Under Transient Frequency Deviation Constraint

The transient frequency deviation is governed jointly by system inertia and frequency-regulation capability. The maximum transient frequency deviation occurs at the instant when generation and load first re-establish power balance after the disturbance, as illustrated in Fig. 3.

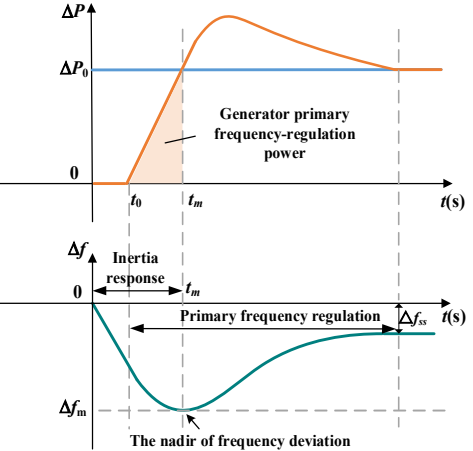


Fig. 3. Frequency response to a step disturbance.

The SFR model is an important tool for predicting frequency dynamics following a disturbance. The equivalent single-machine representation, including the participation of power electronic units, is shown in Fig. 4.

The time at which the maximum frequency deviation occurs and the corresponding maximum deviation are given by:

$$t_m = \frac{1}{\omega_r} \tan^{-1} \left( \frac{\omega_r T_R}{\zeta \omega_n T_R - 1} \right) \tag{19}$$

$$\Delta f_m = \frac{R\Delta P_0}{K_{L_{SVS}}R + 1} \cdot \left[1 + \sqrt{1 - \zeta^2} \alpha e^{-\zeta \omega_n t_m}\right]$$
 (20)

where  $K_{Lsys} = K_L + K_n K_W$ ,  $H_{sys} = H + K_n K_v / 2$ ;  $K_n$  is the proportion of

new energy units, and  $K_V$  is the virtual inertia coefficient. The meanings of the other variables and their detailed expressions can be found in [5].

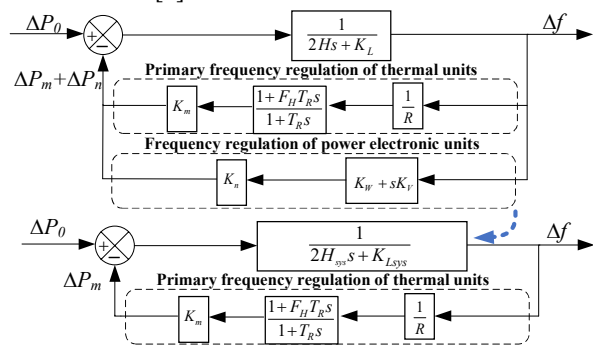


Fig. 4. SFR model with participation of power electronic units.

On this basis, the maximum disturbance power that the system can tolerate under the transient frequency deviation constraint is obtained as:

$$\Delta P_{\text{max 3}} = \frac{\Delta f_{\text{max}} (K_{L_{Sys}} R + 1) S_N}{R (1 + \sqrt{1 - \zeta^2} \alpha e^{-\zeta \omega_n t_m})}$$
(21)

Comparing the maximum tolerable disturbance powers derived from the steady-state and transient constraints, the overall critical disturbance power is determined as:

$$\Delta P_{max} = min\{\Delta P_{\text{max}1}, \Delta P_{\text{max}2}, \Delta P_{\text{max}3}\}$$
 (22)

To evaluate the severity of a step disturbance and visualize the remaining frequency stability margin, a safety-margin indicator is introduced as:

$$\eta = \frac{\Delta P_{\text{max}} - \Delta P_0}{\Delta P_{\text{max}}} \tag{23}$$

When  $0 < \eta < 1$ , the system frequency remains stable and a smaller value of  $\eta$  indicates a smaller safety margin. When  $\eta < 0$ , the system becomes unstable and a more negative value of  $\eta$  corresponds to a more severe frequency event.

# C. Second-Level Slope Disturbance

Once a second-level slope disturbance is identified, the time required for the frequency deviation to reach the transient limit is relatively short. The SFR model can therefore be used to compute the time at which the frequency deviation reaches its limit, based on the transient frequency deviation constraint. The frequency response induced by a second-level slope disturbance is shown in Fig. 5.

When the disturbance power varies linearly with time and the disturbance inception is taken as the time origin, it can be expressed as  $\Delta P_0 = k_s t$ . The modified SFR model for a ramp disturbance in the complex domain can then be written as:

$$\Delta f(s) = \frac{k_s T_1 T_2 R \omega_n^2}{K_{Lsys} R + 1} \left( \frac{1 + T_R s}{s^2 (1 + T_1 s) (1 + T_2 s)} \right)$$
(24)

where 
$$T_1 = \frac{\zeta + \sqrt{\zeta^2 - 1}}{\omega_n}$$
,  $T_2 = \frac{\zeta - \sqrt{\zeta^2 - 1}}{\omega_n}$ 

Applying the inverse Laplace transform to (24), the timedomain expression of the frequency deviation is obtained as:

$$\Delta f(t) = \frac{k_s R}{K_{Lsys} R + 1} \left( t + T_R - T_1 - T_2 + k_1 e^{-t/T_1} + k_2 e^{-t/T_2} \right) (25)$$

where 
$$k_1 = \frac{T_1^2 - T_R T_1}{T_1 - T_2}$$
,  $k_2 = \frac{T_2^2 - T_R T_2}{T_2 - T_1}$ .

Let  $t_{\rm m}$  denote the time when the transient frequency deviation first reaches its limit value  $\Delta f_{\rm max}$ . Substituting  $\Delta f(t) = \Delta f_{\rm max}$  and  $t = t_{\rm m}$  into (25) yields:

$$\frac{\Delta f_{\text{max}}(K_{Lsys}R+1)}{k_{o}R} - T = t_{m} + k_{1}e^{-t_{m}/T_{1}} + k_{2}e^{-t_{m}/T_{2}}$$
 (26)

where  $T=T_R-T_1-T_2$ .

Solving (26) gives the over-limit time of frequency deviation under second-level slope disturbances.

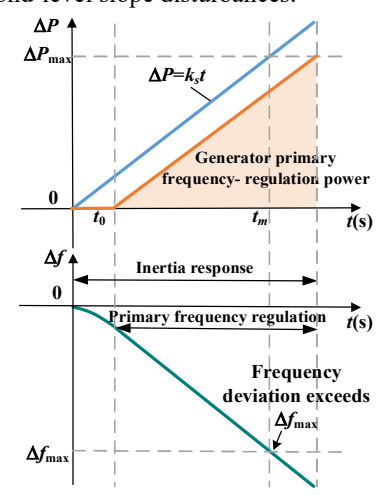


Fig. 5. Frequency response caused by a second-level slope disturbance.

### D. Minute-level Slope Disturbances

For minute-level slope disturbances, the time required for the frequency deviation to reach its transient limit is much longer than for the other two types of disturbances. The corresponding frequency response is shown in Fig. 6.

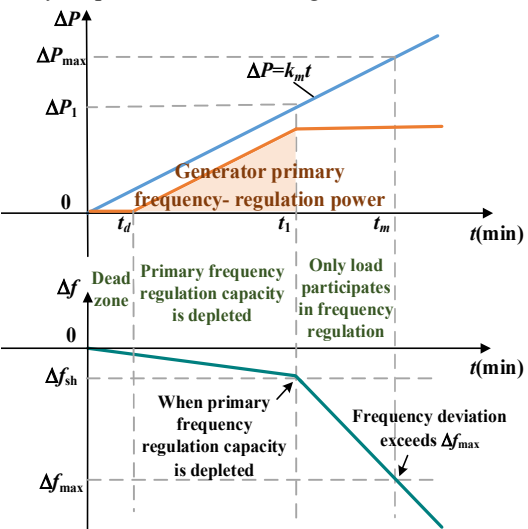


Fig. 6. Frequency response caused by a minute-level slope disturbance.

The frequency evolution can be divided into two stages. Before  $t_1$ , the primary frequency regulation of generators and loads acts cooperatively, and the system operates at a new quasi-steady-state operating point. At  $t_1$ , primary frequency-regulation capacity of the generators is exhausted. After  $t_1$ , only load-frequency regulation remains effective, and the frequency

deviation deteriorates rapidly.

The generator rotor motion equation is:

$$\begin{cases} \frac{\mathrm{d}\delta}{\mathrm{d}t} = \omega - \omega_{N} \\ \frac{\mathrm{d}\omega}{\mathrm{d}t} = \frac{\Delta M}{T_{J}} \approx \frac{\Delta P_{m} - \Delta P_{e}}{T_{J}} \end{cases}$$
 (27)

where  $T_J$  is the system inertia time constant  $(T_J=2H_{sys})$ ;  $\delta$  is the angle between the generator rotor q-axis and the real axis of the synchronous reference frame;  $\Delta P_m$  is the unbalanced mechanical power;  $\Delta P_e$  is the unbalanced electromagnetic power;  $\omega$  is the rotor angular speed; and  $\omega_N$  is the nominal angular speed.

For  $t > t_1$ , the primary frequency-regulation capability of the generators has been fully utilized:

$$\begin{cases}
\Delta P_m = 0 \\
\Delta P_e = \Delta P + \Delta P_L
\end{cases}$$
(28)

After  $t_1$ , the additional power imbalance produced by the continuously increasing disturbance power is:

$$\Delta P = k_m (t - t_1) \tag{29}$$

Combining (28) and (29) results in:

$$\Delta P = -(T_{\rm J} \cdot \frac{\mathrm{d}\Delta f}{\mathrm{d}t} + K_{Lsys}\Delta f) \tag{30}$$

Equation (30) is a first-order linear non-homogeneous differential equation. Its general solution for the frequency deviation is:

$$\Delta f(t) = Ce^{-K_{Lsys}t/T_{J}} + \frac{k_{m}}{K_{Lsys}} (t_{1} - t + \frac{T_{J}}{K_{Lsys}})$$
 (31)

At  $t=t_1$ , the incremental frequency deviation caused by the newly generated power imbalance is zero, which determines the integration constant C as:

$$C = -e^{K_{L_{Sys}}t_1/T_J} \frac{k_m T_J}{K_{L_{Sys}}^2}$$
 (32)

Substituting (32) into (31), and noting that the steady-state frequency deviation at this time has already reached  $\Delta f_{\rm sh}$ , the frequency response after  $t_1$  can be expressed as:

$$\Delta f(t) = -\frac{k_m T_J}{K_{Lsys}^2} e^{K_{Lsys}(t_1 - t)/T_J} + \frac{k_m}{K_{Lsys}} (t_1 - t + \frac{T_J}{K_{Lsys}}) + \Delta f_{sh}$$
 (33)

Replacing  $\Delta f(t)$  and t by  $\Delta f_{max}$  and  $t_m$ , respectively, the time  $t_m$  at which the frequency deviation reaches its limit can be obtained using numerical methods. This gives the over-limit time of frequency deviation under minute-level slope disturbances.

# E. Flowchart of Quantitative Discriminant Method for Frequency Stability Control

The specific implementation steps for quantitative discrimination of frequency stability under unanticipated disturbances are summarized as follows, and the overall procedure is illustrated in Fig. 7.

# 1) Short-term and step disturbances

Once a short-term or step disturbance is identified, the disturbance power  $\Delta P_0$  is obtained from the generator and disturbance-point voltage measurements using (3) – (6). The maximum tolerable disturbance power  $\Delta P_{\text{max}}$  is then calculated

from the transient frequency deviation constraint for short-term disturbances by (16) and from the steady-state and transient constraints for step disturbances by (17) – (22). Comparing  $\Delta P_0$  with  $\Delta P_{\rm max}$  determines whether the system frequency remains within the prescribed limits.

### 2) Second-level slope disturbances

For a second-level slope disturbance, the disturbance ramp rate  $k_s$  is first evaluated using (7) and (8). The values of  $k_s$  and the transient frequency-deviation limit  $\Delta f_{\rm max}$  are then substituted into the ramp-type SFR model (24) – (26) to compute the time  $t_{\rm m}$  at which the frequency deviation reaches its limit. This overlimit time provides a quantitative indicator of the frequency stability margin under second-level slope disturbances.

# 3) Minute-level slope disturbances

For a minute-level slope disturbance, the disturbance ramp rate  $k_m$  at the frequency threshold is obtained from the power-balance condition using (9) – (11) together with the thresholds defined in (1) and (2). Based on the rotor motion equation and its solution in (27) – (33), the time  $t_m$  for the frequency deviation to reach its limit is then predicted. This allows the operator to assess how long the system can withstand a slowly evolving disturbance before violating the frequency-security constraints.

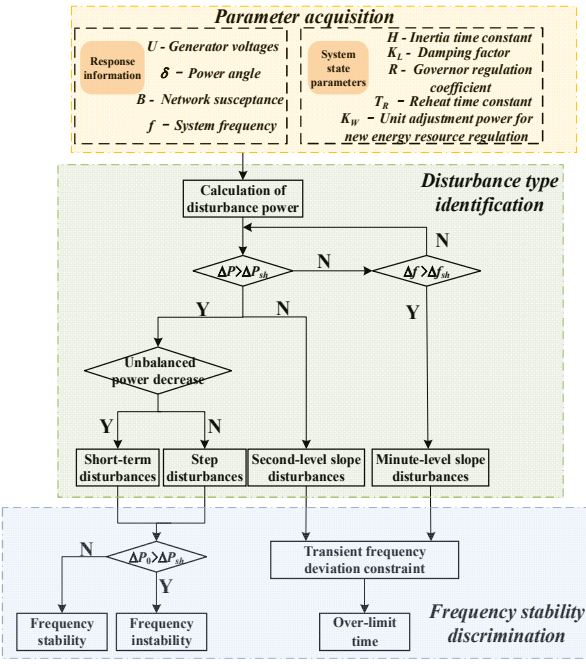


Fig. 7. Flow chart of response-based quantitative frequency stability assessment under unanticipated disturbances.

## V. CASE STUDIES AND VERIFICATION

# A. Test System Description

This section validates the proposed response-based quantitative frequency-stability assessment method using the frequency-stability benchmark system developed by the China Electric Power Research Institute (CSEE-FS) [25]. The benchmark represents a realistic AC- DC hybrid power system with 47 buses, 31 ac transmission lines and three  $\pm 500~\rm kV$  HVDC links. The generation portfolio consists of seven conventional units with a total installed capacity of 5400 MW (3400 MW thermal and 2000 MW hydropower) and 6900 MW

of renewable generation (wind and photovoltaic), so that the installed share of renewables reaches 56.1%. The total active load is 4852.1 MW. The main 500 kV backbone network and the locations of conventional and renewable plants are shown in Fig. 8.

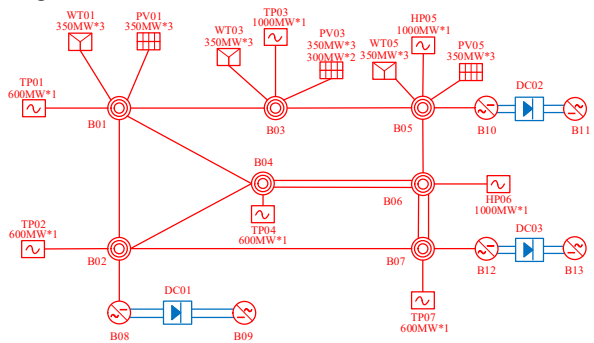


Fig. 8. System topology of CSEE-FS.

The low-frequency operating scenario is selected as the base operating point. The equivalent system inertia time constant and load-frequency damping coefficient are  $T_J$  = 2.68 s and  $K_L$  = 2.0, respectively. The aggregated SFR parameters are chosen as  $H_{\rm sys}$  = 1.34s,  $K_{\rm w}$  = 3, R=0.05,  $K_{\rm Lsys}$ =3,  $F_{\rm H}$ =0.3, and  $T_{\rm R}$ =10s. The primary frequency-regulation limits of conventional generators and renewables are both set to m=6% and n=6% of their respective online capacities, and the unbalanced-power distribution time at the onset of a disturbance is taken as T = 0.5 s. For minute-level slope disturbances, the critical disturbance-power slope is set to  $k_1$ =7.3MW/s, hence, the disturbance-power threshold and the frequency deviation threshold are  $\Delta P_{\rm sh}$ = 3.65MW and  $\Delta f_{\rm sh}$ =0.33Hz, respectively.

### B. Verification of Short-Term Disturbances

The proposed method is verified using the PSD-BPA simulation software. Three groups of operating conditions are established, as summarized in Table II. The LVRT duration is set to 0.4 s, 0.5 s, and 0.6 s, respectively, and the active-power recovery rate of the renewable plant is  $K_R$ =2000MW/s. According to (16), when the admissible maximum transient frequency deviation is set to  $|\Delta f_{\rm max}|$ =0.75Hz, the maximum disturbance powers that the system can tolerate under the transient frequency deviation constraint are calculated to be 1380.2 MW, 1253.8 MW and 1143.8 MW for the three LVRT durations, respectively.

At t=1.0s, a three-phase fault is applied to the 500 kV transmission line between buses B03 and B05 of the CSEE-FS system. The LVRT control of PV03 is activated, causing its active power to drop temporarily and resulting in a power deficit of  $\Delta P_0$ =1350MW. The disturbance power  $\Delta P_0$  evaluated by (6) exceeds  $\Delta P_{\rm sh}$  and rapidly returns to zero after fault clearing, which is consistent with the definition of a short-term disturbance. The LVRT duration is set according to operating conditions 1–3 in Table II. Supported by system inertia, kinetic energy is continuously converted into electrical power, leading to a continuous decline in system frequency during the LVRT interval. After the disturbance is cleared, the system exhibits almost no steady-state frequency deviation.

TABLE II

MAXIMUM TOLERABLE DISTURBANCE POWER AND MAXIMUM TRANSIENT
FREQUENCY DEVIATION UNDER DIFFERENT LVRT DURATIONS

Operating condition	LVRT duration (ms)	Maximum tolerable disturbance power (MW)	Maximum transient frequency deviation (Hz)
1	400	1380.2	-0.543
2	500	1253.8	-0.789
3	600	1143.8	-0.892

For operating conditions 1–3, the maximum transient frequency deviations are 0.543 Hz, 0.789 Hz, and 0.892 Hz, respectively. Under a 1350 MW short-term disturbance, the system can maintain frequency stability only when the LVRT duration is 0.4 s. The active power of PV03-1 and the system frequency response are shown in Fig. 9 and Fig. 10, respectively.

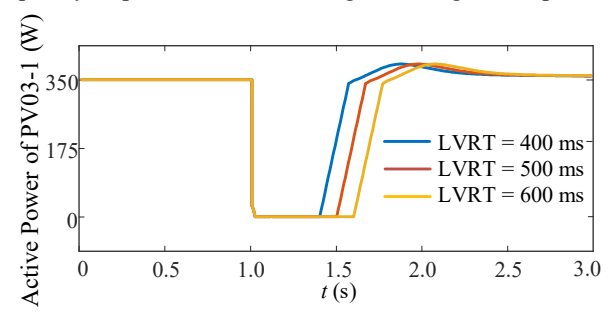


Fig. 9. Active power of PV03-1 under different LVRT durations.

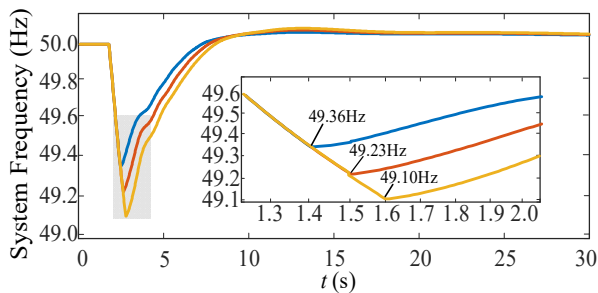


Fig. 10. System frequency response under different LVRT durations.

# C. Verification of Step Disturbances

For step disturbances, the steady-state frequency-deviation limit is set to  $|\Delta f_{ss}|$ =0.2Hz, and the maximum transient frequency deviation limit is kept at  $|\Delta f_{max}|$ =0.75Hz. According to (17) and (18), the critical disturbance powers under the steady-state constraint are 398.8MW and 362.8MW, respectively. From (21), the corresponding critical disturbance power under the transient constraint is 647.6MW. Therefore, the overall critical disturbance power is  $\Delta P_{max}$ =362.8MW.

To verify this result, step load-increase disturbances of 350 MW, 520 MW, and 690 MW are applied at t=1.0s at bus B01. During the power-distribution interval, the disturbance power  $\Delta P$  computed from (6) remains constant and exceeds  $\Delta P_{\rm sh}$  in all three cases, confirming that they are step disturbances. Comparing  $\Delta P$  with  $\Delta P_{\rm max}$  shows that the 520 MW disturbance causes the steady-state frequency deviation to exceed its limit, while the 690 MW disturbance causes both the peak transient frequency deviation and the steady-state deviation to exceed their respective thresholds. In contrast, the 350 MW disturbance leaves the system marginally stable. The system frequency response is shown in Fig. 11.

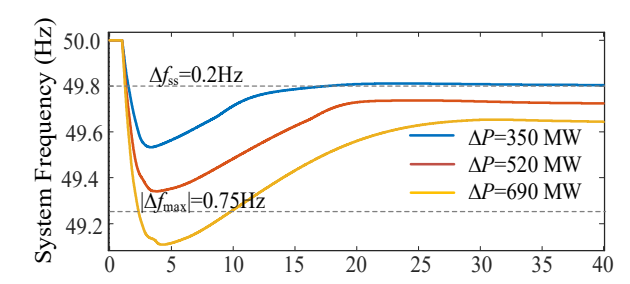


Fig. 11. System frequency response under different step-disturbance powers.

The corresponding frequency deviations and safety-margin indicators, summarized in Table III, indicate a small positive margin (3.53%) for the 350 MW case and negative margins for the 520 MW and 690 MW cases, with the 690 MW disturbance exhibiting a margin of –90.19%, i.e., significantly exceeding the critical power threshold. These results are consistent with the theoretical analysis and confirm the effectiveness of the proposed criterion for step-disturbance assessment.

TABLE III
FREQUENCY DEVIATIONS AND STABILITY MARGIN UNDER DIFFERENT STEPDISTURBANCE POWERS

Disturbance power (MW)	Maximum transient frequency deviation (Hz)	Steady-state frequency deviation (Hz)	Stability margin (%)
350	-0.47	-0.19	3.53
520	-0.66	-0.28	-43.33
690	-0.89	-0.36	-90.19

### D. Verification of Second-level Disturbances

To emulate a second-level slope disturbance, the DC transmission power is commanded to vary linearly starting at t=0.5s, resulting in a total power change of 600MW over 10 s. During the initial power-distribution interval, the disturbance power  $\Delta P$  computed from (6) increases approximately linearly with time and exceeds the threshold  $\Delta P_{\rm sh}$  at t=60.8ms, thereby confirming that the event is classified as a second-level slope disturbance. The corresponding disturbance-power slope is  $k_{\rm s}$ =60MW/s, obtained from (8). For a transient frequency-deviation limit of  $\Delta f_{\rm max}$ , the proposed analytical model yields a predicted over-limit time of  $t_m$ =13.13s. Table IV lists the disturbance-power slope and the predicted and simulated over-limit times.

TABLE IV

COMPARISON BETWEEN PREDICTED AND SIMULATED OVER-LIMIT TIMES FOR
A SECOND-LEVEL SLOPE DISTURBANCE

A SECOND LEVEE SEGIE DISTORBANCE				
Disturbance-power	Predicted over-	Simulated over-	Relative	
slope	limit time	limit time	error	
(MW/s)	(s)	(s)	(%)	
60	13.13	13.65	3.81	

Fig. 12 compares the frequency response predicted by the proposed method with the time-domain simulation results. The red curve represents the detailed simulation of the CSEE-FS system, while the blue curve denotes the response calculated using the ramp-type SFR model. In the simulation, the frequency deviation reaches  $|\Delta f_{\rm max}|$ =0.75Hz at t=13.65s, corresponding to a relative error of 3.81% with respect to the predicted value. This close agreement indicates that the proposed method can accurately identify second-level slope disturbances and reliably predict the time at which the

frequency deviation exceeds the prescribed limit.

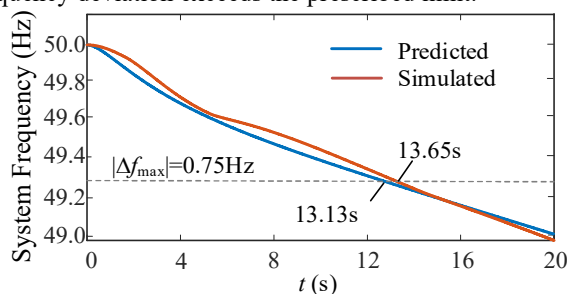


Fig. 12. System frequency response to a second-level slope disturbance: comparison between predicted and simulated results.

## E. Verification of Minute-Level Slope Disturbances

To verify the case of a minute-level slope disturbance, the DC transmission power is commanded to vary linearly starting at t=1s, resulting in a total power reduction of 1800MW over 1000s. According to (6), during the initial power-distribution interval the disturbance power  $\Delta P$  increases approximately linearly and reaches 0.9MW at t=0.5s which is lower than the power threshold  $\Delta P_{\rm sh}$ . Hence, the disturbance cannot be classified as a step or second-level slope disturbance.

At  $t_1$ =140.1s, the frequency deviation reaches the starting threshold  $\Delta f_{\rm sh}$ , at which point the event is identified as a minute-level slope disturbance. The corresponding disturbance-power slope is  $k_{\rm m}$ =0.9MW/s, obtained from (11). For a transient frequency-deviation limit of  $|\Delta f_{\rm max}|$ =0.75Hz, the proposed analytical model yields a predicted over-limit time of  $t_m$ =248.7s, as calculated from (33). Table V summarizes the disturbance-power slope and the predicted and simulated over-limit times.

TABLE V

COMPARISON BETWEEN PREDICTED AND SIMULATED OVER-LIMIT TIMES FOR A MINUTE-LEVEL SLOPE DISTURBANCE

_	A MINOTE LEVEE BEGIE BISTORBANCE			
-	Disturbance-power	Predicted over-	Simulated over-	Relative
	slope	limit time	limit time	error
	(MW/s)	(s)	(s)	(%)
	0.90	248.7	255.2	2.55

Fig. 13 compares the frequency response predicted by the proposed minute-level slope disturbance model with the time-domain simulation results. The red curve represents the simulated response, while the blue curve denotes the trajectory obtained from the analytical model. In the simulation, the frequency deviation reaches -0.75Hz at t=255.2s, corresponding to a relative error of only 2.55% with respect to the predicted over-limit time. This close agreement confirms that the proposed algorithm can accurately identify minute-level slope disturbances and reliably predict the over-limit time.

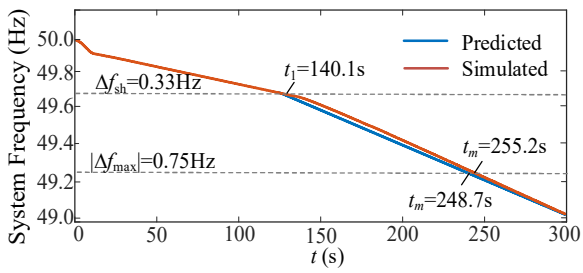


Fig. 13. System frequency response to a minute-level slope disturbance: comparison between predicted and simulated results.

### VI. CONCLUSION

This paper has developed a response-based quantitative frequency-stability assessment method that unifies the treatment of different disturbance types and time scales in high-renewable power systems. The main findings are as follows.

- 1) Unified disturbance classification and intensity metrics. Using generator electrical response data, unanticipated disturbances are classified into short-term disturbances, step disturbances, second-level slope disturbances and minute-level slope disturbances. Disturbance power and disturbance-power slope are used as unified indicators of disturbance intensity. A power threshold derived from the critical slope separates step and second-level slope disturbances, while a frequency-deviation threshold associated with the exhaustion of primary frequency regulation is used to identify minute-level slope disturbances.
- 2) Analytical criteria for frequency stability. For step disturbances, analytical expressions are derived for the maximum tolerable disturbance power under both transient and steady-state frequency-deviation constraints, and a safety-margin index is introduced to visualize the remaining frequency-stability margin. For second-level and minute-level slope disturbances, the SFR model and the rotor motion equation after primary frequency regulation has been exhausted are used to obtain closed-form frequency responses and to compute the over-limit time of frequency deviation.
- 3) Validation on the CSEE-FS benchmark system. Case studies on the CSEE-FS frequency-stability benchmark system under typical LVRT, step-load and DC ramp disturbances show that the proposed method can accurately identify disturbance types, quantitatively characterize disturbance intensity, and predict the time at which the frequency deviation exceeds its limit with small errors. These results demonstrate that the proposed response-based framework provides a practical tool for online frequency-stability assessment and active prevention and control in high-renewable power systems.

### REFERENCES

- M. Rezkalla, M. Pertl, and M. Marinelli, "Electric power system inertia: Requirements, challenges and solutions," *Electrical Engineering*, vol. 100, pp. 2677–2693, Aug. 2018.
- [2] F. Milano, F. Dörfler, G. Hug, D. J. Hill, and G. Verbič, "Foundations and challenges of low-inertia systems," in *Proceedings of the 2018 Power Systems Computation Conference (PSCC)*, 2018, pp. 1–25.
- [3] D. Liu, X. Zhang, and C. K. Tse, "Effects of high level of penetration of renewable energy sources on cascading failure of modern power systems," *IEEE Transactions on Emerging and Selected Topics in Circuits and Systems*, vol. 12, no. 1, pp. 98–106, Mar. 2022.
- [4] M. H. Athari and Z. Wang, "Impacts of wind power uncertainty on grid vulnerability to cascading overload failures," *IEEE Transactions on Sustainable Energy*, vol. 9, no. 1, pp. 128–137, Jan. 2018.
- [5] P. M. Anderson and M. Mirheydar, "A low-order system frequency response model," *IEEE Transactions on Power Systems*, vol. 5, no. 3, pp. 720–729, Aug. 1990.
- [6] M. Krpan and I. Kuzle, "Introducing low-order system frequency response modelling of a future power system with high penetration of wind power plants with frequency support capabilities," *IET Renewable Power Generation*, vol. 12, no. 13, pp. 1453–1461, Apr. 2018.
- [7] I. Egido, F. Fernandez-Bernal, P. Centeno, and L. Rouco, "Maximum frequency deviation calculation in small isolated power systems," *IEEE Transactions on Power Systems*, vol. 24, no. 4, pp. 1731–1738, Nov. 2009.

- [8] F. Teng, Y. Mu, H. Jia, J. Wu, P. Zeng, and G. Strbac, "Challenges on primary frequency control and potential solution from EVs in the future GB electricity system," *Applied Energy*, vol. 194, pp. 353–362, May 2017.
- [9] P. M. Ashton, C. S. Saunders, G. A. Taylor, A. M. Carter, and M. E. Bradley, "Inertia estimation of the GB power system using synchrophasor measurements," *IEEE Transactions on Power Systems*, vol. 30, no. 2, pp. 701–709, Mar. 2015.
- [10] B. Wang, Y. Liu, Y. Liu, Z. Hu, and Z. Chen, "Power system inertia estimation method based on maximum frequency deviation," *IET Renewable Power Generation*, vol. 16, no. 3, pp. 622–633, Feb. 2022.
- [11] M. García-Ruiz, G. J. Cantos-Alcántara, J. L. Martínez-Ramos, and A. Marano-Marcolini, "Minimum required inertia for a fully renewable AC interconnected system," in Proceedings of the 2019 International Conference on Smart Energy Systems and Technologies (SEST), 2019, pp. 1–6.
- [12] J. Morren, S. W. H. de Haan, W. L. Kling, and J. A. Ferreira, "Wind turbines emulating inertia and supporting primary frequency control," *IEEE Transactions on Power Systems*, vol. 21, no. 1, pp. 433–434, Feb. 2006
- [13] C. Pradhan, C. N. Bhende, and A. K. Samanta, "Adaptive virtual inertiabased frequency regulation in wind power systems," *Renewable Energy*, vol. 115, pp. 558–574, Jan. 2018.
- [14] H. Gu, R. Yan, and T. K. Saha, "Minimum synchronous inertia requirement of renewable power systems," *IEEE Transactions on Power Systems*, vol. 33, no. 2, pp. 1533–1543, Mar. 2018.
- [15] P. Kundur, Power System Stability and Control. New York, NY, USA: McGraw-Hill, 1994.
- [16] Y. Yuan, Y. Zhang, J. Wang, Z. Liu, and Z. Chen, "Enhanced frequency-constrained unit commitment considering variable-droop frequency control from converter-based generator," *IEEE Transactions on Power Systems*, vol. 38, no. 2, pp. 1094–1110, Mar. 2023.
- [17] National Grid Electricity System Operator (ESO), "Technical report on the events of 9 August 2019," Sep. 2019. [Online]. Available: https://www.nationalgrideso.com/document/152346/download
- [18] National Grid Electricity System Operator (ESO), "Appendices to the technical report on the events of 9 August 2019," Sep. 2019. [Online]. Available:
  - https://www.nationalgrideso.com/document/152351/download
- [19] Y. Huo, Y. Xu, C. Shen, Z. Wang, and C. Wan, "Data-driven coordinated voltage control method of distribution networks with high DG penetration," *IEEE Transactions on Power Systems*, vol. 38, no. 2, pp. 1543–1557, Mar. 2023.
- [20] Y. Cai, X. Wang, G. Joós, and I. Kamwa, "An online data-driven method to locate forced oscillation sources from power plants based on sparse identification of nonlinear dynamics (SINDy)," *IEEE Transactions on Power Systems*, vol. 38, no. 3, pp. 2085–2099, May 2023.
- [21] H. Li, S. You, Z. Jiang, J. Tan, A. Hoke, J. Liu, L. Zhu, B. Rockwell, C. Kruse, and Y. Liu, "Ambient-frequency-data based system-level inertia estimation using physical equation and its practice on Hawaii Islands," *IEEE Transactions on Power Systems*, vol. 39, no. 6, pp. 6948–6959, Sep. 2024.
- [22] F. Hong, Y. Pang, W. Ji, L. Liang, and F. Fang, "Assessment and enhancement of frequency response capability of power systems considering thermal power dynamic conditions," CSEE Journal of Power and Energy Systems, vol. 10, no. 4, pp. 1371–1383, Jul. 2024.
- [23] H. He, N. Zhang, C. Kang, S. Ci, F. Teng, and G. Strbac, "Communication resources allocation for time delay reduction of frequency regulation service in high renewable penetrated power system," CSEE Journal of Power and Energy Systems, vol. 10, no. 2, pp. 468–480, Mar. 2024.
- [24] Y. Xie, S. Ma, J. Shen, X. Tang, J. Ren, and L. Zheng, "Wide-area active frequency control with multi-step-size model predictive control," CSEE Journal of Power and Energy Systems, vol. 11, no. 3, pp. 972–986, May 2025.
- [25] H. Sun, B. Zhao, S. Xu, T. Lan, Z. Li, and P. Wu, "Test models for stability/security studies of AC–DC hybrid power systems with high penetration of renewables," *IEEE Transactions on Power Systems*, vol. 40, no. 1, pp. 957–969, Jan. 2025.